Polymer Infused Porous Surfaces for Robust, Thermally Conductive, Self-Healing Coatings for Dropwise Condensation

Polymer Infused Porous Surfaces (PIPS) for Robust, Thermally Conductive, Self-Healing Coatings for Dropwise Condensation

Kyle L. Wilke[1], *Dion S. Antao*[1,†], *Samuel Cruz*[1], *Ryuichi Iwata*[1,2], *Yajing Zhao*[1], *Arny Leroy*[1], *Daniel J. Preston*[1,††], *Evelyn N. Wang*[1,*]

[1]Department of Mechanical Engineering, Massachusetts Institute of Technology, Cambridge, MA 02139, USA

[2]Toyota Central R&D Labs., Inc., Nagakute, Aichi, 480-1192, Japan

Present Addresses

[†]J. Mike Walker '66 Department of Mechanical Engineering, Texas A&M University, College Station, TX 77843, USA

[††]Department of Mechanical Engineering, Rice University, 6100 Main St., Houston, TX 77005, USA

Corresponding Author: *enwang@mit.edu

TOC Figure

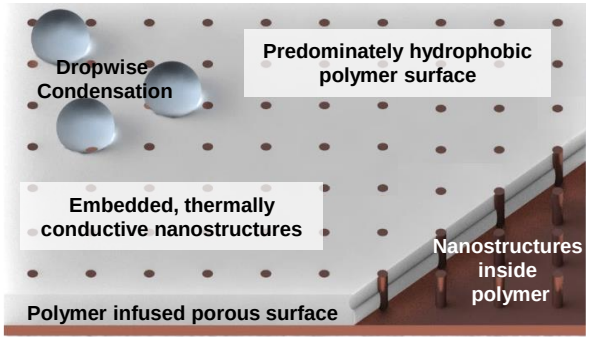

Abstract

Hydrophobic coatings with low thermal resistance promise a significant enhancement in condensation heat transfer performance by promoting dropwise condensation in applications including power generation, water treatment, and thermal management of high-performance electronics. However, after nearly a century of research, coatings with adequate robustness remain elusive due to the extreme environments within many condensers and strict design requirements needed to achieve enhancement. In this work, we enable long-lasting condensation heat transfer enhancement *via* dropwise condensation by infusing a hydrophobic polymer, Teflon AF, into a porous nanostructured surface. This polymer infused porous surface (PIPS) uses the large surface area of the nanostructures to enhance polymer adhesion, while the nanostructures form a percolated network of high thermal conductivity material throughout the polymer and drastically reduce the thermal resistance of the composite. We demonstrate over 700% enhancement in the condensation of steam compared to an uncoated surface. This performance enhancement was sustained for more than 200 days without significant degradation. Furthermore, we show that the surfaces are self-repairing upon raising the temperature past the melting point of the polymer, allowing recovery of hydrophobicity, offering a level of durability more appropriate for industrial applications.

Keywords: condensation, heat transfer, self-healing, hydrophobic, nanostructure, polymer, thermally conductive coatings

Tailoring wetting behavior during condensation can greatly enhance heat transfer performance for applications including power generation,[1-3] water purification,[4-6] and thermal management.[7-9] In fact, the majority of electricity in the United States is produced with steam cycle power plants in which the condensation of water plays a critical role.[10] Industrial condensers are typically manufactured from metals that are highly wetting to water, leading to the filmwise mode of condensation in which the condensate forms a thick liquid film of large thermal resistance on the condenser surface and impedes heat transfer. Conversely, upon rendering the surface of a condenser hydrophobic with a low-surface-energy coating, the condensate forms discrete droplets that nucleate, grow, coalesce, and easily shed in the dropwise mode of condensation.[11] Because condensate is removed from the surface more efficiently, heat and mass transfer performance can be improved by an order of magnitude by transitioning from filmwise to dropwise condensation, which consequently improves overall steam cycle efficiency.[3]

Despite the fact that low-surface-energy coatings for condensation enhancement have been explored for nearly a century,[12-25] industry continues to rely on filmwise condensation, primarily due to a lack of durable coatings. Prior work has focused on developing numerous types of low-surface-energy coatings including monolayer promoters,[17,26-29] organic films,[22-24,30,31] lubricant infused surfaces (LIS)[32-35] including LIS where additional lubricant is continuously added using a brush to increase lifetime,[36] and graphene.[25] Recent work has also focused on combining these coatings with surface structuring to further enhance hydrophobicity and achieve jumping-droplet condensation.[21,37-40] However, robust coatings that achieve significant performance enhancement have not yet been demonstrated (Figure 1). Instead, adequate lifetimes of organic coatings were only achieved when the coating thickness was large (>4 μm),[23] and, due to the large thermal resistance of the coatings, the thickness of these coatings significantly reduced the performance

enhancement. Thinner coatings of various types, which achieved significant performance enhancement, failed quickly.[23,24] Two studies remain inconclusive due to short testing periods (1-3 weeks) that did not show coating failure, graphene coatings and thin polymers deposited using initiated chemical vapor deposition (iCVD). Studies that did not test to failure are denoted in Figure 1 with a single asterisk and include an arrow pointing to the right to represent the possibility of higher robustness. The heat transfer enhancement of graphene was limited, likely due to relatively large contact angle hysteresis of the surfaces leading to large condensate droplet departure diameters, while the iCVD coating process may present the opportunity to be used in combination to the strategies employed in this work to further improve performance of both approaches. Meanwhile, other forms of enhancement without low-surface-energy coatings have focused on increased heat transfer area through the use of extended surfaces,[41] wicking to promote condensate removal,[42,43] and fluid-repellent surface structuring that relies only on geometric effects.[44] Unfortunately, the heat transfer enhancement demonstrated with these methods has not been as impressive as strategies incorporating low-surface-energy coatings.

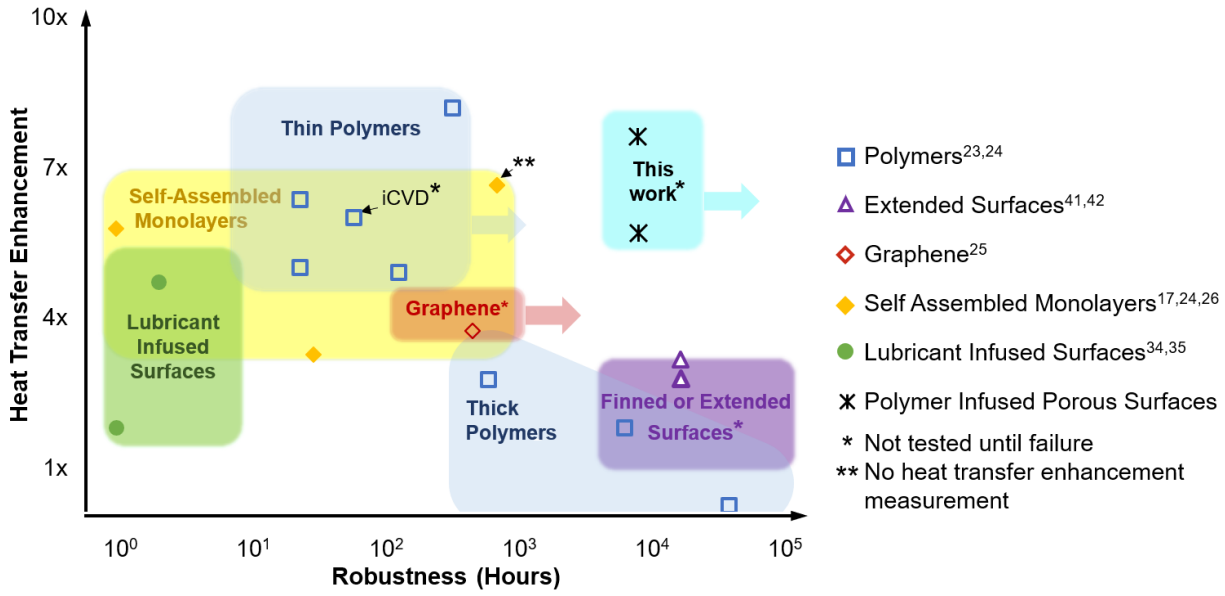

Figure 1: Robustness and Performance. Heat transfer enhancement compared to filmwise condensation and observed robustness (lifetime) of various hydrophobic surface coatings including lubricant infused surfaces,[34,35] monolayer promoters,[17,24,26] polymers,[23,24] graphene,[25] and finned and extended surfaces.[41,42] Coatings that achieve large improvements in performance are thin, limiting heat transfer resistance through the coating but causing the coatings to fail quickly. On the other hand, thick, robust coatings and finned surfaces exhibit minimal performance enhancement. The PIPS introduced in this work achieved both a large enhancement and a long lifetime. (Note that each referenced work may use different condensation conditions, resulting in additional variance in observed enhancement and robustness. All data shown is for condensation of water. Enhancement for other liquids may follow different trends.)

In this work, we demonstrate an approach to address both the large thermal resistance and poor robustness of hydrophobic coatings simultaneously. A hydrophobic polymer (Teflon AF) was infused into nanostructures grown directly on condenser surfaces. The nanostructures create a large surface area for adhesion and constrain the polymer to the surface, improving durability. Furthermore, because the nanostructures create a percolated network of high thermal conductivity

material through the low thermal conductivity polymer, the thermal resistance of the coating is greatly reduced. We discuss the design and fabrication of these polymer infused porous surfaces (PIPS) and demonstrate dropwise condensation for more than 200 days with heat transfer performance 5.9-7.5× higher than that of filmwise condensation (Figure 1). We also show that coatings of this type are self-healing upon raising the temperature of the surface above the polymer melting point, allowing simple recovery of the initial hydrophobicity if degradation or damage does occur.

Results/Discussion

Design of PIPS. To achieve durable condensation heat transfer enhancement through dropwise condensation with low-surface-energy coatings, multiple design criteria for the proposed PIPS were considered (see Supporting Information S1 and Figure S1 for greater detail). First, the thermal resistance needs to be sufficiently low as to not impede heat transfer. This resistance scales as H/k, where H is the thickness of the coating and k is the thermal conductivity (Figure S2b). Therefore, a low resistance was achieved by using the porous nanostructures embedded into the polymer to enhance thermal conductivity while keeping the overall thickness sufficiently thin. In this work, we adopt the naming convention nanostructure solid fraction to describe the ratio of nanostructure to polymer. This convention was chosen given that before infusion of polymer, the nanostructure is porous and solid fraction accurately describes the amount of nanostructure relative to void space to be filled by polymer. Second, the coating must enable dropwise condensation. Generally, the quality and performance of dropwise condensation is greatest when the advancing contact angle, θ_a, is large ($\theta_a > 90$ degrees) and the contact angle hysteresis, *i.e.*, the difference between the advancing contact angle and the receding contact angle, is small ($\theta_a - \theta_r < 20$ degrees).[45] The hysteresis is reduced by keeping the nanostructure solid fraction at the surface

exposed to condensate as low as possible. Therefore, the optimal nanostructure solid fraction can be determined from a balance of increasing effective thermal conductivity and keeping contact angle hysteresis low (Figure S1b). Finally, coating adhesion must be large enough to prevent delamination of the polymer,[23,46] which was achieved by utilizing nanostructures with high surface area to mechanically interlock, constrain, and adhere the polymer to the surface (Figure S1c).[47-49]

Fabrication of PIPS. Based on the design considerations above, nanostructures were chosen that could be controlled within appropriate nanostructure solid fraction and thickness for significant heat transfer enhancement (blue highlighted rows of Table S1). These nanostructures represent significantly different designs while still promising enhancement, demonstrating the flexibility of PIPS. Specifically, we chose copper oxide nanoblades and copper nanowires (Figure 2a) due to the ability to grow them directly on the condenser surfaces with dimensions in the required range (details of fabricated samples in Table 1). In this case, the lower thermal conductivity and varying solid fraction of the copper oxide caused these surfaces to have a lower effective thermal conductivity than those using copper, limiting the thickness used (Table S1).[40,50] Only one thickness of CuO nanoblade PIPS was used due to the self-limiting nature of nanoblade growth (methods). To fabricate PIPS, these nanostructures were grown directly on the condenser surface and then infused with polymer until the entire nanostructure was filled (Figure 2b). Care was taken not to overfill the nanostructures, given overfilling would create a layer of low-thermal-conductivity polymer on top of the nanostructures, creating additional resistance to heat transfer. As seen in Table S1 only 220 nm of Teflon AF without embedded nanostructures would decrease performance by 10 percent, highlighting the importance of preventing overfilling. The polymer Teflon AF 1600 was chosen for its hydrophobicity and the ease of filling the nanostructure due to its high surface wettability in solution. By spin coating consecutive layers of Teflon AF, the filling

was precisely controlled and stopped before overfilling (Figure 2c). Scanning electron microscope images, water contact angle measurements, and atomic force microscopy were used to determine when filling was complete. After spin coating, the surface was heated above the polymer melting point to ensure proper filling of the nanostructure without voids. This resulted in a predominately Teflon AF surface with very low roughness, ideal for enabling dropwise condensation, as shown in Figure 2d with atomic force microscope images of a copper oxide surface at the filling stages in Figure 2c.

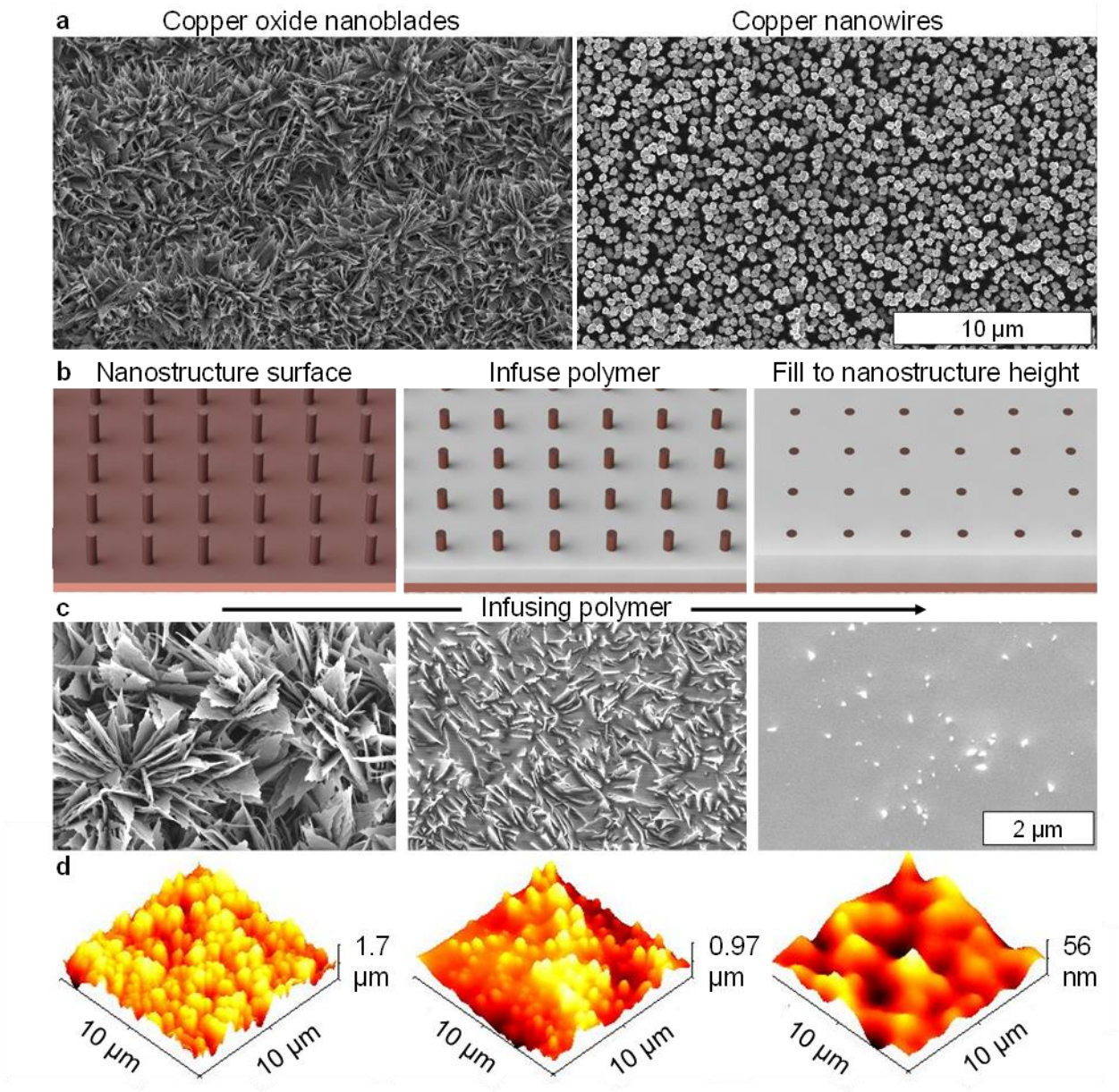

Figure 2: Fabrication of PIPS. a, Top view scanning electron microscope images of copper oxide nanoblades and copper nanowires used in this study. Scale bar for both images. **b**, Generalized 3D schematic of the fabrication process for PIPS, where the nanostructures are represented by pillars. First, nanostructures are grown directly on the condenser surface. Next, the polymer is infused until the nanostructure is completely filled without covering the surface with additional polymer to prevent additional resistance to heat transfer. **c**, Top view scanning electron microscope images

of filling copper oxide nanostructures at different stages. Filling was stopped when the polymer completely filled the structure, but had not yet formed a layer on top of the nanostructure. Scale bar is for all images. **d**, Atomic force microscope images as the nanostructure was infused. The final surface had very small roughness, resulting in a smooth hydrophobic surface (note the relatively small vertical scale).

Table 1: Properties of fabricated surfaces. The geometry and measured advancing and receding contact angles of all surfaces used in this study. These geometries were chosen to test a range of designs that were expected to provide enhancement using standard fabrication methods. 2 μm and 20 μm Teflon AF coatings with no nanostructure were also fabricated on bare copper as reference. Note the copper surface had an oxide layer that was not removed before coating. $\phi(x = 0)$ is the nanostructure solid fraction at the surface exposed to condensate. Note that the uncertainty in the contact angle measurement is 5°.

Nanostructure / Polymer	$\boldsymbol{H}$ **[μm]**	$\boldsymbol{\phi(x = 0)}$	$\boldsymbol{\theta_a}$ **[deg]**	$\boldsymbol{\theta_r}$ **[deg]**
- / Teflon AF	2	0	107.2	106
- / Teflon AF	20	0	106.7	105
Cu Nanowires / Teflon AF	5	0.4	108	92
Cu Nanowires / Teflon AF	20	0.4	105.1	89
CuO Nanoblades / Teflon AF	1.5	~0	108.2	103.2

Heat Transfer Coefficient Testing. The resulting surfaces consisted predominantly of Teflon AF. This resulted in a high quality, hydrophobic surface with large advancing contact angle and low contact angle hysteresis (Table 1), where hysteresis is larger on the Cu nanowire surfaces due to the larger nanostructure solid fraction of nanostructure at the surface. These surfaces were tested

under conditions typical in a power plant condenser.[51] An environmental chamber (Figure 3a) was used to control a pure vapor ambient for condensation. Experiments were run at ~60 °C saturated vapor conditions and a heat flux of 100 kW/m2 was applied to the surfaces. This temperature and heat flux are representative of conditions in an industrial condenser. All surfaces, including PIPS, were fabricated directly on copper rods connected to a chiller loop, allowing accurate control over the condensation heat flux applied to the surfaces. Thermocouples embedded in the copper rod were used to extrapolate the heat flux as well as the heat transfer coefficient (Supporting Information S2). This chamber allowed for simultaneous visualization of surfaces and monitoring of heat transfer performance during testing.

The heat transfer coefficient (HTC) of dropwise condensation, h_c, on the low thermal resistance PIPS was comparable to that observed in the literature for previously developed thin, non-robust coatings for dropwise condensation (Figure 3b). The shaded region shows the expected performance of dropwise condensation at the tested conditions using a correlation developed by Rose based on experimental measurements of heat transfer at various temperatures and heat fluxes (133-142 kW/m^2-K predicted), while the filmwise performance was measured to be ~16 kW/m^{2}K on a bare copper condenser, close to the expected performance calculated using Nusselt Film Theory.[52] The model lines show the expected performance including the added thermal resistance of the different PIPS coatings (Supporting Information S3). Because Cu nanowire PIPS has reduced thermal resistance compared to both the CuO nanoblade PIPS and the Teflon AF, the overall thickness could be increased significantly without decreasing heat transfer performance, whereas a Teflon AF-only coating significantly reduced performance at a thickness of only 2 micrometers. In fact, PIPS with Cu nanowires demonstrated heat transfer performance near that expected of dropwise condensation even at thicknesses up to 20 μm, whereas a Teflon AF only

coating this thick had performance worse than filmwise condensation. This behavior is expected based on the large predicted effective thermal conductivity and critical thickness of Cu nanowire PIPS in Supplemental Information S1 and Table S1. The observed values for PIPS tended to be less than the expected values based on modeling (lines in Figure 3), although within the uncertainty. We attribute this discrepancy to three factors: first, the equations that we used to estimate effective thermal conductivity of PIPS tend to overpredict the true value,[53,54] particularly for less ordered structures such as CuO nanoblades; second, although care was taken to not overfill the Teflon AF in the nanostructures, any overfilling that does occur would reduce dropwise heat transfer performance due to the additional thermal resistance the overfilling creates; finally, the heat transfer coefficient of dropwise condensation adopted to create the shaded dropwise region and establish the modeling lines for expected performance while varying thickness is based on previous studies of dropwise condensation, but the performance of a particular surface is dependent on various parameters, such as nucleation density and contact angle hysteresis (Supplemental Information S4).

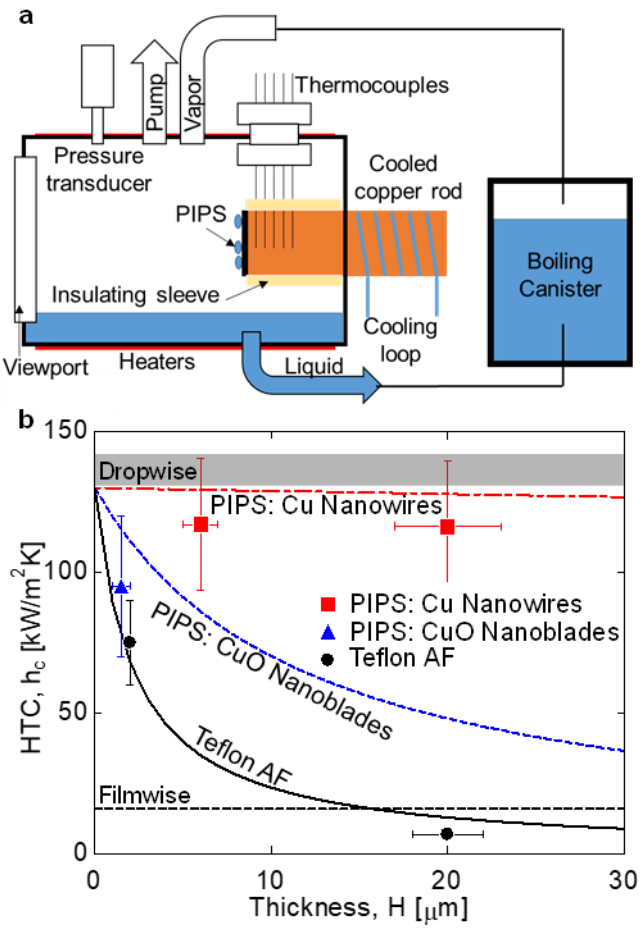

Figure 3: Heat Transfer Testing of PIPS. a, Schematic of environmental chamber for heat transfer coefficient and durability testing of PIPS. A pure vapor ambient was maintained at controlled conditions. PIPS were fabricated directly on copper rods cooled by a chiller, inducing condensation on the surface at a controlled heat flux. A viewport allowed imaging of the surface. **b**, Measured condensation heat transfer coefficient. PIPS achieved performance similar to other state of the art coatings for dropwise condensation. However, due to the reduced thermal resistance, performance was not significantly reduced as coating thickness of PIPS with copper nanowires is increased, providing design flexibility. Compared to similar thicknesses of Teflon AF without embedded nanostructures, performance was significantly higher.

Durability Testing. The 20 μm thick Cu nanowire PIPS, the CuO nanoblade PIPS, and the 2 μm Teflon AF coating, all of which showed enhancement over filmwise condensation, were then tested for robustness by continuously condensing on the surface at ~60 °C saturated vapor conditions and a heat flux of ~100 kW/m^2. To ensure a pure water vapor ambient, vacuum was pulled on the system once per week to remove any buildup of non-condensable gases (see Methods: Continuous Condensation Testing). The heat transfer coefficient of the 2 μm Teflon AF coating started with a 4.7× enhancement over filmwise condensation, but degradation of performance started within hours (Figure 4a). This degradation was caused by delamination of the Teflon AF, resulting in a film of water forming in the delaminated regions (Figure 4b) and ultimately resulting in complete failure within 100 hours, a consistent degradation mechanism with previous works.[23,46] We note there are strategies to moderately improve lifetime before failure for polymer coatings on bare surfaces that we did not pursue in this work.[55] PIPS, however, did not show any significant degradation based both on the heat transfer measurement and the surface imaging after 4800+ hours of testing (Figure 4a and b). After testing the CuO Nanoblade PIPS contact angles and contact angle hysteresis remained unchanged, while hysteresis on the Cu Nanowire PIPS increased from 16.1 degrees to 28.5 degrees (Figure 4c). This was not due to delamination of the polymer. Rather, we attribute this increase in hysteresis to the larger nanostructure solid fraction of the Cu Nanowire PIPS resulting in a larger sensitivity to nanostructure becoming exposed and/or surface roughness increasing as degradation at the surface occurs (Supporting Information S4 and Figure S5). We believe it may also be in part because CuO nanoblade PIPS are more resistant to corrosion than Cu nanowire PIPS (Supporting Information S5 and Table S2); however, the exact degradation mechanism is not known. An increase in contact angle hysteresis would typically result in a decrease in heat transfer coefficient, whereas here an

apparent increase was observed. However, we note that all changes were within the uncertainty of the measurement and no reliable conclusion can be made. Furthermore, even though an increase in contact angle hysteresis would typically cause a decrease in performance, other factors, such as an increase in nucleation density due to surface degradation, could in fact result in an increase in performance (Supplementary Information S4).

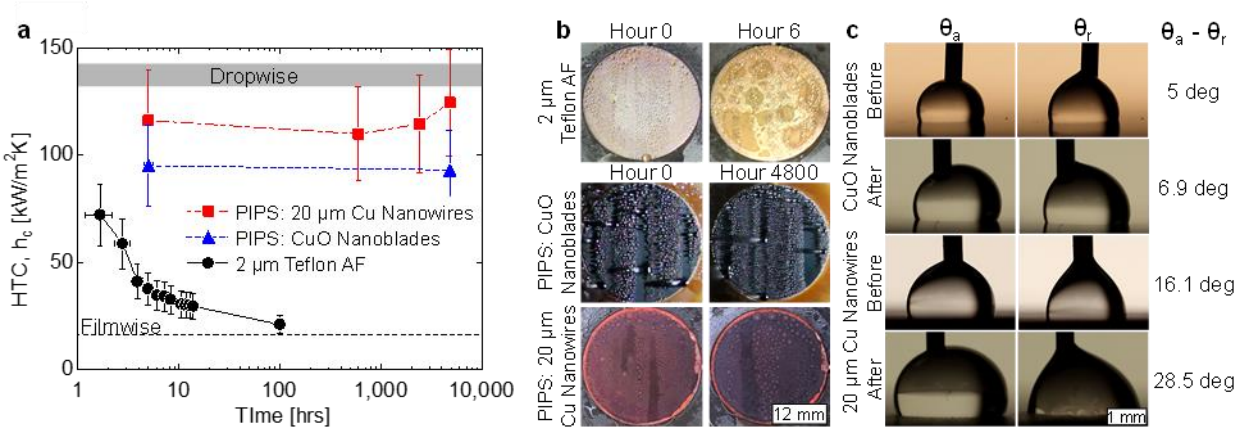

Figure 4: Durability of PIPS. a, The heat transfer coefficient, HTC, on 20 µm Cu nanowire PIPS, CuO nanoblade PIPS, and 2 µm Teflon AF during continuous condensation of steam. Teflon AF performance degrades within 100 hours, while both PIPS show little to no degradation for 200+ days. The apparent increase of HTC for the Cu Nanowire PIPS over time is not considered significant given it also falls within uncertainty. Data for PIPS does not start at 1 hour because HTC was averaged over an extended period to reduce experimental uncertainty due to fluctuations in chamber conditions caused by PID control. **b**, The mode of degradation of the Teflon AF surface is delamination of the coating, which can be seen in the image after 6 hours. PIPS, on the other hand, continues to exhibit high-quality dropwise condensation even after 200+ days. Videos S1 – S4 show condensation on PIPS at different times. **c**, The contact angles and contact angle hysteresis of CuO nanoblade PIPS was unchanged after 4800+ hours of testing. Hysteresis on Cu Nanowire PIPS, however, increased by 12 degrees. This was not enough to make an observable change to

the dropwise condensation performance in Figure 4a and b; however, it is expected that continued degradation would decrease performance. Uncertainty in contact angle measurements was 5 degrees.

Self-Healing. The continuous condensation study demonstrated the increased durability of PIPS, with no degradation observed on CuO nanoblade PIPS and minor degradation of contact angle on Cu Nanowire PIPS with little to no effect on heat transfer performance. However, continued degradation or incidental mechanical damage would be expected to reduce performance. Therefore, we also demonstrate that, because the surface was prepared using a polymer that can melt, a simple mechanism for self-healing exists. Self-healing surfaces are generally split into two categories: autonomic, which heal automatically when damaged, and non-autonomic, which require an external trigger to heal, such as heat or light.[56,57] PIPS fall into the second category, where applying heat to re-flow the polymer repairs damage to the polymer due to capillary effects reducing surface roughness. By heating the surface to 330 °C for 30 minutes, the contact angle hysteresis on the 20 μm Cu nanowire PIPS tested for more than 200 days is once again reduced, as shown in Figure 5a. The ability of this surface to heal suggests that the increase in contact angle hysteresis was unlikely due to removal of any significant amount of Teflon AF from the surface, given without the Teflon AF the surface would not properly heal. Rather, it suggests the surface degradation resulted in an increase in surface roughness or exposed nanostructure in a way that healing was able to remove the roughness or reduce the amount of exposed nanostructure. To further demonstrate self-healing, we intentionally damaged surfaces more significantly than what was observed in durability testing with a variety of methods. Figure 5b shows a CuO nanoblade PIPS damaged using laser ablation. The laser, which was used to create a grid of damaged lines on the surface, created roughly 100 μm wide damaged sections where the polymer was largely

removed from the embedded nanoblades. However, during self-healing the polymer reflowed and repaired the surface, thereby recovering the original wetting properties. In Figure 5c, the advancing and receding contact angles of damaged and repaired CuO nanobloade PIPS are shown. The advancing contact angle is the upper bound of the box, whereas the receding contact angle is the lower bound. The original, undamaged surface was hydrophobic with small hysteresis. The surface was then damaged in different ways. Laser ablation, as shown in Figure 5b, removed much of the polymer but did not completely destroy the underlying nanostructure; scraping using a multiblade cross hatch cutting tool (ISO 2409:2007) destroyed both the polymer, nanostructure, and underlying surface; and chemical damage (achieved here by placing the surface in an oxygen plasma for 3 minutes) removed fluorination (and thus hydrophobicity) at the surface of the coating but left the underlying polymer and structure undamaged.[58] After repair, the original contact angles were largely recovered for all types of damage, where the level of physical damage to the surface and nanostructure determined how well the surface could be repaired. Because chemical damage did not destroy the structure at all, the original contact angles were completely recovered, whereas with scraping, which caused significant damage to the surface, the wetting properties were only partially recovered. The recovery of surface wetting properties and dropwise condensation behavior is demonstrated in Figure 5d. The white lines in Figure 5d are the grid of laser damage. Due to the large contact angle hysteresis of the damaged surface, droplets on the surface grow large and begin to spread, covering the surface. However, after repair, small, highly mobile droplets and dropwise condensation were once again achieved due to the recovery of original wetting properties.

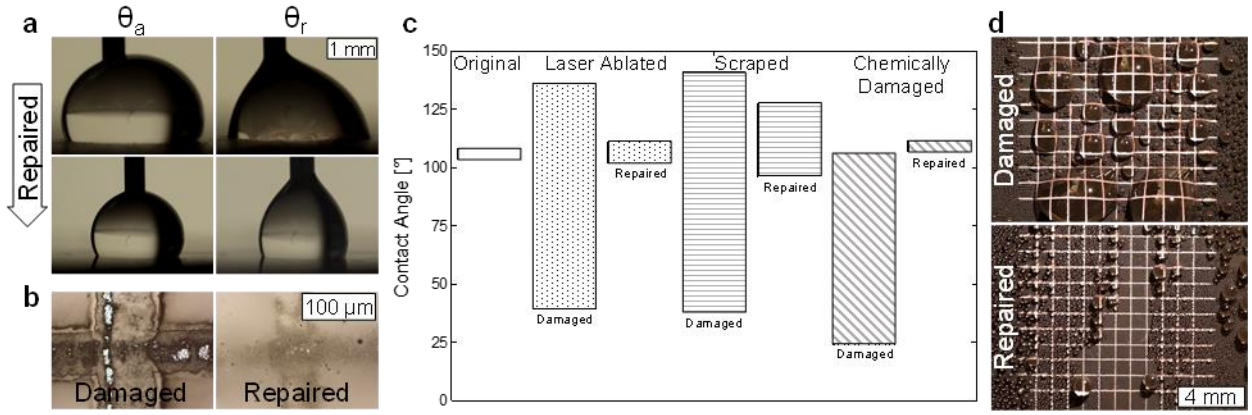

Figure 5: Self-Healing of PIPS. a, After 4800+ hours of testing, the contact angle hysteresis on Cu Nanoblade PIPS had increased (top row). However, after self-healing by heating, θ_a was 111.1 degrees and θ_r was 101 degrees, reducing hysteresis greatly and returning the surface to its original state before degradation. **b**, Left shows a Cu Nanoblade PIPS surface damaged by laser ablation. The laser removed polymer from the surface and partially destroyed the nanostructure. However, by heating the surface past the melting point of the polymer, the surface largely self-healed (right). **c,** Advancing and receding contact angle of a Cu Nanoblade PIPS surface. Advancing angle is the upper bound of the bar, whereas receding is the lower bound. Uncertainty in contact angle measurements was 5 degrees. After damage of various types, contact angle hysteresis was significantly increased. However, after healing, the original wetting properties are largely recovered. Scraping, *i.e.*, significant damage to the surface and nanostructure, recovered the least. **d**, Condensation on damaged PIPS and repaired PIPS for the laser ablated surface. The damaged surface has large droplets due to the large contact angle hysteresis. After repair high quality dropwise condensation is recovered.

Conclusions. Based on the demonstrated combination of heat transfer performance and lifetime of PIPS, the coating enables a regime of surface wetting-based enhancement not previously achieved (Figure 4a), where adequate lifetimes were demonstrated without sacrificing heat transfer

enhancement. This enhancement was achieved by creating PIPS that address the typical challenges associated with using low-surface-energy coatings. The composite surfaces we developed (Figure 2), consisting of a high-thermal conductivity nanostructure filled with a hydrophobic polymer, create a predominately polymer surface. This approach renders the surface hydrophobic, while the nanostructures embedded within the polymer enhance the thermal conductivity, not only reducing constraints on the coating thickness but also greatly enhancing the adhesion of the coating for improved lifetime. Furthermore, the choice of nanostructure and polymer allow the surface to be self-healing *via* heating. Not only are PIPS robust, high performance coatings, but they can also be easily repaired to damage that does not significantly destroy the nanostructures or underlying condenser surface. This enabled a combination of heat transfer performance and lifetime more appropriate for industrial condensers, promising enhancement of applications including power generation, water treatment, and thermal management of high-performance electronics.

Methods/Experimental

Fabrication of Surfaces

The fabrication procedure for PIPS is shown in Figure 2. Each step is described in further detail here.

Growth of CuO Nanoblades

The copper surfaces were first polished (SCRUBS Metal Polish Towel), cleaned with detergent (Alconox Detergent Powder), placed in an ultrasonic bath with isopropanol for 10 min, rinsed with deionized (DI) water, placed in 2 M hydrochloric acid for 30 seconds, rinsed with DI water, and then dried with compressed air. CuO nanoblades were then grown by immersing the cleaned rods

in alkaline solution composed of $NaClO_2$, NaOH, $Na_3PO_4 \cdot 12H_2O$, and DI water (3.75:5:10:100 wt %) at 96 °C for 1 hour. Based on literature characterization of this oxidation process and atomic force microscopy images, the CuO nanoblades have thickness of $h \approx 1.5$ μm, nanostructure solid fraction at the surface $\phi(x = 0) \approx 0.023$, and surface area enhancement of ≈ 10.[37] The random orientation of the nanoblades also physically constrains the polymer to the surface, *i.e.*, in order to delaminate the polymer coating must be significantly deformed. This growth process is self-limiting, thus thicker CuO nanoblades could not be made with this process.

Growth of Cu Nanowires

Copper nanowires were grown using a two-step templated electrodeposition process. The copper surfaces were first polished (SCRUBS Metal Polish Towel), cleaned with detergent (Alconox Detergent Powder), placed in an ultrasonic bath with isopropanol for 10 min, rinsed with deionized (DI) water, placed in 2 M hydrochloric acid for 30 seconds, rinsed with DI water, and then dried with compressed air. A 50 μm thick anodized aluminum oxide nanoporous membrane 200 nm pore diameter and nanostructure solid fraction of ≈ 0.4 (Sterlitech) was placed on the copper surface. In the first electrodeposition step, a piece of filter paper was then placed on top of the membrane and wetted with electrolyte (Elevate Cu Electrolyte 10). Finally, a piece of copper the same size as the surface (1 in diameter disk) was placed on top of the filter paper. The entire stack was clamped together and placed in the electrolyte. A constant current was then applied (2.5 mA for InRedox templates, 10 mA for Sterlitech templates) for one hour to bond the template to the copper surface. The clamp, filter paper, and second piece of copper were removed, leaving only the template bonded to the copper sample surface. The sample was then placed back into the electrolyte for the second electrodeposition step. A constant current was applied (2.5 mA for

InRedox templates, 10 mA for Sterlitech templates), where the electrodeposition time controlled the thickness of the nanowire layer. A growth rate of 1.5 μm – 2 μm per hour was observed. After the desired thickness was reached, the surface was removed from the electrolyte, rinsed with DI water, and placed in 2 M NaOH solution for 3 hr to remove the AAO, leaving copper nanowires behind.

Infusion of Teflon AF

After growth of CuO nanoblades or Cu nanowires, Teflon AF 1601 (6% solution, Chemours) was spin coated on the surfaces at 1000 rpm. Spin coating allows controlled thicknesses to be deposited.[59] After spin coating, the surface was heated in argon to 330 °C with a ramp rate of 30 °C per minute, held at 330 °C for 30 minutes, and then allowed to cool to room temperature. This heating process allowed the spin coated layer to melt, and wick into the nanostructured surface. This spin coating process was then repeated until the nanostructure was completely filled, *i.e.*, the number of spin coats was changed depending on nanostructure thickness and nanostructure solid fraction, where each spin coat deposited ≈ 1 μm of Teflon AF or less. When the nanostructure was nearly filled the thickness deposited was reduced to ≈ 100 nm each spin coat by using a diluted solution (3%) of Teflon AF 1601 to prevent overfilling.

Contact Angle Measurements

A custom-built experimental setup was used to measure contact angle (Figure S6a). The air and liquid temperature remained close to the surrounding laboratory temperature. A syringe pump (Micro4, World Precision Instruments) was used to add and remove water from a droplet on the surface. Note that the liquid was added and removed slowly enough that there was no dynamic

effect on the contact angle, *i.e.*, the capillary number was small. A DSLR camera (EOS Rebel T3, Cannon) and macro lens were used to collect images of the droplet advancing on the surface. Lighting of the droplet was supplied with a light source (Intenselight C-HGFI, Nikon) and lens (C-HGFIB, Nikon). Contact angle was extracted from the images using ImageJ. Due to the lack of precise control over the orientation of the surface relative to the camera and the use of uncollimated lighting, the uncertainty in the contact angle measurement was 5 degrees.

Self-Healing: Damage and Repair

The PIPS surface was damaged in three different ways. First was laser ablation using a commercial laser cutter (Epilog Laser Zing 24). The laser power was set to 15% and cutting speed to 100%. The laser cutter then produced a 10x10 grid of lines spaced 1 mm apart. This removed the polymer but did not completely destroy the nanostructure. Scraping was achieved using a multiblade cross hatch cutting tool (ISO 2409:2007), which destroyed both the polymer and nanostructure. Chemical damage was achieved by placing the surface in a plasma chamber (790 series, Plasmatherm) for 3 minutes, which removed fluorination (and thus hydrophobicity) at the surface of the coating but left the underlying polymer and structure undamaged.[58]

Corrosion Testing

The potentiodynamic polarization curves were measured in 1 liter of 3.5 weight percent NaCl solution. 1 cm^2 surfaces were used for the tests. The surface was first allowed to sit in the solution for 15 minutes before starting the test. Voltage was then swept at a rate of 0.1 mV/s from 250 mV below to 250mV above the open circuit voltage and the current monitored. Using Tafel extrapolation, the corrosion current was then determined.[60]

Continuous Condensation Testing

Before condensation testing, all thermocouples (ungrounded J-type, Omega) were calibrated to ±0.1 °C in a water bath (Lauda recirculating chiller). Surfaces for testing were prepared directly on 1 inch diameter copper rods that extended through the walls of an environmental chamber (schematic of chamber in Figure 3a and picture in Figure S6b). These rods were connected to a chilling loop, which was used to set condensation heat flux. The copper rods were insulated by a 0.25" thick plastic sleeve to prevent condensation on any surface but PIPS. While some condensation on the insulating sleeves did still occur, modeling in Comsol shows it does not significantly impact the measurement (Supplemental Information S2). Furthermore, condensate from the insulating sleeve was not observed to fall directly onto the PIPS sample, and therefore does not affect droplet shedding behavior (Supplemental Videos S1-4). The environmental chamber was evacuated to less than 1 Pa to remove all non-condensable gases. Steam was then added *via* a boiler filled with degassed DI water. Steam conditions were set to 60 °C by heaters in the boiler, and the chamber walls were maintained at this temperature using heaters applied directly to the chamber walls. Steam temperature was monitored by 5 thermocouples. Chiller temperature was set to produce roughly 100 kW/m^2 heat flux at the condenser surface, extrapolated from temperatures measured by 5 thermocouples embedded along the length of the copper cylinder. Fitting the temperature profile in the copper cylinder also allowed the surface subcooling, and condensation heat transfer coefficient, to be calculated. For long term testing, vacuum was pulled on the chamber once per week to ensure non-condensable gases did not accumulate over time.

Associated Content

Supporting Information.

The following files are available free of charge on the ACS Publications website at DOI:

Description of the design of PIPS, the heat transfer measurement and expected performance, contact angle hysteresis, corrosion resistance, and uncertainty propagation (PDF)

Video S1 – S4: dropwise condensation on Cu nanowire and CuO nanoblade PIPS on the first day of durability testing and after 200 days of testing at 60 °C with 100 kW/m^2 heat flux (MP4)

A provisional patent has been filed on this work.

Author Information

Corresponding Author

*enwang@mit.edu

Author Contributions

K.L.W. and E.N.W conceived the idea of PIPS. K.L.W. and S.C. fabricated samples. K.L.W. tested the samples. D.S.A. designed the environmental testing chamber. A.L. did heat transfer modeling of samples. D.S.A. and D.J.P. provided guidance on design and testing. R.I. and K.L.W. did the corrosion testing. K.L.W. and Y.Z. did heat transfer modeling. E.N.W. guided the work. The manuscript was written through contributions of all authors. All authors have given approval to the final version of the manuscript.

Acknowledgment

This work was supported by the Cooperative Agreement between the Masdar Institute of Science and Technology (Masdar Institute), Abu Dhabi, UAE and the Massachusetts Institute of Technology (MIT), Cambridge, MA, USA - Reference 02/MI/MIT/CP/11/07633/GEN/G/00. The authors acknowledge funding for this research from the Electric Power Research Institute (EPRI)

under award number 00-10002062, with Dr. Jessica Shi as Program Manager. R.I. acknowledges the support from TOYOTA CENTRAL R&D LABS., INC.

References

1. Beér, J. M. High Efficiency Electric Power Generation: The Environmental Role. *Prog. Energy Combust. Sci.* **2007,** *33*, 107-134.

2. Glicksman, L. R.; Hunt Jr, A. W. Numerical Simulation of Dropwise Condensation. *Int. J. Heat Mass Transfer* **1972,** *15*, 2251-2269.

3. Schilling, H. Improving the Efficiency of Pulverised Coal Fired Power Generating Plant. *VGB Kraftwerkstech.* **1993,** *73*, 564-576.

4. Humplik, T.; Lee, J.; O'hern, S.; Fellman, B.; Baig, M.; Hassan, S.; Atieh, M.; Rahman, F.; Laoui, T.; Karnik, R. Nanostructured Materials for Water Desalination. *Nanotechnology* **2011,** *22*, 292001, 1-19.

5. Andrews, H.; Eccles, E.; Schofield, W.; Badyal, J. Three-Dimensional Hierarchical Structures for Fog Harvesting. *Langmuir* **2011,** *27*, 3798-3802.

6. Khawaji, A. D.; Kutubkhanah, I. K.; Wie, J.-M. Advances in Seawater Desalination Technologies. *Desalination* **2008,** *221*, 47-69.

7. Leach, R.; Stevens, F.; Langford, S.; Dickinson, J. Dropwise Condensation: Experiments and Simulations of Nucleation and Growth of Water Drops in a Cooling System. *Langmuir* **2006,** *22*, 8864-8872.

8. Peters, T. B.; McCarthy, M.; Allison, J.; Dominguez-Espinosa, F. A.; Jenicek, D.; Kariya, H. A.; Staats, W. L.; Brisson, J. G.; Lang, J. H.; Wang, E. N. Design of an Integrated Loop Heat Pipe Air-Cooled Heat Exchanger for High Performance Electronics. *IEEE Trans. Compon., Packag., Manuf. Technol.* **2012,** *2*, 1637-1648.

9. Cho, H. J.; Preston, D. J.; Zhu, Y.; Wang, E. N. Nanoengineered Materials for Liquid–Vapour Phase-Change Heat Transfer. *Nat. Rev. Mater.* **2017,** *2*, 16092, 1-17.

10. Wiser, W. H. Electric Power. *Energy Resources: Occurrence, Production, Conversion, Use*, Springer Science & Business Media: New York, 2012; pp 183-198.

11. Rose, J. Dropwise Condensation Theory and Experiment: A Review. *Proc. Inst. Mech. Eng., Part A* **2002,** *216*, 115-128.

12. Penniman, A. L. Surface Condenser. 1992504, 26 Feb., 1935.

13. Drew, T.; Nagle, W.; Smith, W. The Conditions for Dropwise Condensation of Steam. *Trans. Am. Inst. Chem. Eng.* **1935,** *31*, 605-621.

14. Nagle, W. U.; Bays, G.; Blenderman, L.; Drew, T. Heat-Transfer Coefficients During Dropwise Condensation of Steam. *Trans. Am. Inst. Chem. Eng.* **1935,** *31*, 593-621.

15. Schmidt, E.; Schurig, W.; Sellschopp, W. Versuche Über Die Kondensation Von Wasserdampf in Film-Und Tropfenform. *Tech. Mech. Thermodyn.* **1930,** *1*, 53-63.

16. Fitzpatrick, J.; Baum, S.; McAdams, W. Dropwise Condensation of Steam on Vertical Tubes. *Trans. Am. Inst. Chem. Eng.* **1939,** *35*, 97-107.

17. Blackman, L.; Dewar, M.; Hampson, H. An Investigation of Compounds Promoting the Dropwise Condensation of Steam. *J. Appl. Chem.* **1957,** *7*, 160-171.

18. McCormick, J.; Westwater, J. Nucleation Sites for Dropwise Condensation. *Chem. Eng. Sci.* **1965,** *20*, 1021-1036.

19. Umur, A.; Griffith, P. Mechanism of Dropwise Condensation. *J. Heat Transfer* **1965,** *87*, 275-282.

20. Kollera, M.; Grigull, U. Über Das Abspringen Von Tropfen Bei Der Kondensation Von Quecksilber. *Wärme-und Stoffübertragung* **1969,** *2*, 31-35.

21. Boreyko, J. B.; Chen, C.-H. Self-Propelled Dropwise Condensate on Superhydrophobic Surfaces. *Phys. Rev. Lett.* **2009,** *103*, 184501, 1-4.

22. Marto, P.; Looney, D.; Rose, J.; Wanniarachchi, A. Evaluation of Organic Coatings for the Promotion of Dropwise Condensation of Steam. *Int. J. Heat Mass Transfer* **1986,** *29*, 1109-1117.

23. Holden, K.; Wanniarachchi, A.; Marto, P.; Boone, D.; Rose, J. The Use of Organic Coatings to Promote Dropwise Condensation of Steam. *J. Heat Transfer* **1987,** *109*, 768-774.

24. Paxson, A. T.; Yagüe, J. L.; Gleason, K. K.; Varanasi, K. K. Stable Dropwise Condensation for Enhancing Heat Transfer *via* the Initiated Chemical Vapor Deposition (ICVD) of Grafted Polymer Films. *Adv. Mater.* **2014,** *26*, 418-423.

25. Preston, D. J.; Mafra, D. L.; Miljkovic, N.; Kong, J.; Wang, E. N. Scalable Graphene Coatings for Enhanced Condensation Heat Transfer. *Nano Lett.* **2015,** *15*, 2902-2909.

26. Vemuri, S.; Kim, K.; Wood, B.; Govindaraju, S.; Bell, T. Long Term Testing for Dropwise Condensation Using Self-Assembled Monolayer Coatings of N-Octadecyl Mercaptan. *Appl. Therm. Eng.* **2006,** *26*, 421-429.

27. Das, A.; Kilty, H.; Marto, P.; Andeen, G.; Kumar, A. The Use of an Organic Self-Assembled Monolayer Coating to Promote Dropwise Condensation of Steam on Horizontal Tubes. *J. Heat Transfer* **2000,** *122*, 278-286.

28. Chen, L.; Liang, S.; Yan, R.; Cheng, Y.; Huai, X.; Chen, S. N-Octadecanethiol Self-Assembled Monolayer Coating with Microscopic Roughness for Dropwise Condensation of Steam. *J. Therm. Sci.* **2009,** *18*, 160-165.

29. Love, J. C.; Estroff, L. A.; Kriebel, J. K.; Nuzzo, R. G.; Whitesides, G. M. Self-Assembled Monolayers of Thiolates on Metals as a Form of Nanotechnology. *Chem. Rev.* **2005,** *105*, 1103-1170.

30. Ma, X.; Chen, J.; Xu, D.; Lin, J.; Ren, C.; Long, Z. Influence of Processing Conditions of Polymer Film on Dropwise Condensation Heat Transfer. *Int. J. Heat Mass Transfer* **2002,** *45*, 3405-3411.

31. Haraguchi, T.; Shimada, R.; Kumagai, S.; Takeyama, T. The Effect of Polyvinylidene Chloride Coating Thickness on Promotion of Dropwise Steam Condensation. *Int. J. Heat Mass Transfer* **1991,** *34*, 3047-3054.

32. Anand, S.; Paxson, A. T.; Dhiman, R.; Smith, J. D.; Varanasi, K. K. Enhanced Condensation on Lubricant-Impregnated Nanotextured Surfaces. *ACS Nano* **2012,** *6*, 10122-10129.

33. Weisensee, P. B.; Wang, Y.; Qian, H.; Schultz, D.; King, W. P.; Miljkovic, N. Condensate Droplet Size Distribution on Lubricant-Infused Surfaces. *Int. J. Heat Mass Transfer* **2017,** *109*, 187-199.

34. Preston, D. J.; Lu, Z.; Song, Y.; Zhao, Y.; Wilke, K. L.; Antao, D. S.; Louis, M.; Wang, E. N. Heat Transfer Enhancement During Water and Hydrocarbon Condensation on Lubricant Infused Surfaces. *Sci. Rep.* **2018,** *8*, 540, 1-9.

35. Xiao, R.; Miljkovic, N.; Enright, R.; Wang, E. N. Immersion Condensation on Oil-Infused Heterogeneous Surfaces for Enhanced Heat Transfer. *Sci. Rep.* **2013,** *3*, 1988, 1-6.

36. Seo, D.; Shim, J.; Lee, C.; Nam, Y. Brushed Lubricant-Impregnated Surfaces (Blis) for Long-Lasting High Condensation Heat Transfer. *Sci. Rep.* **2020,** *10*, 1-13.

37. Miljkovic, N.; Enright, R.; Nam, Y.; Lopez, K.; Dou, N.; Sack, J.; Wang, E. N. Jumping-Droplet-Enhanced Condensation on Scalable Superhydrophobic Nanostructured Surfaces. *Nano Lett.* **2012,** *13*, 179-187.

38. Enright, R.; Miljkovic, N.; Al-Obeidi, A.; Thompson, C. V.; Wang, E. N. Condensation on Superhydrophobic Surfaces: The Role of Local Energy Barriers and Structure Length Scale. *Langmuir* **2012,** *28*, 14424-14432.

39. Miljkovic, N.; Wang, E. N. Condensation Heat Transfer on Superhydrophobic Surfaces. *MRS Bulletin* **2013,** *38*, 397-406.

40. Enright, R.; Miljkovic, N.; Dou, N.; Nam, Y.; Wang, E. N. Condensation on Superhydrophobic Copper Oxide Nanostructures. *J. Heat Transfer* **2013,** *135*, 091304.

41. Wanniarachchi, A.; Marto, P.; Rose, J. Film Condensation of Steam on Horizontal Finned Tubes: Effect of Fin Spacing. *J. Heat Transfer* **1986,** *108*, 960-966.

42. Preston, D. J.; Wilke, K. L.; Lu, Z.; Cruz, S. S.; Zhao, Y.; Becerra, L. L.; Wang, E. N. Gravitationally Driven Wicking for Enhanced Condensation Heat Transfer. *Langmuir* **2018,** *34*, 4658-4664.

43. Wang, R.; Antao, D. S. Capillary-Enhanced Filmwise Condensation in Porous Media. *Langmuir* **2018,** *34*, 13855-13863.

44. Wilke, K. L.; Preston, D. J.; Lu, Z.; Wang, E. N. Toward Condensation-Resistant Omniphobic Surfaces. *ACS Nano* **2018,** *12*, 11013-11021.

45. Neumann, A.; Abdelmessih, A.; Hameed, A. The Role of Contact Angles and Contact Angle Hysteresis in Dropwise Condensation Heat Transfer. *Int. J. Heat Mass Transfer* **1978,** *21*, 947-953.

46. Ma, X. H.; Wang, B. X.; Xu, D. Q.; Lin, J. F. Lifetime Test of Dropwise Condensation on Polymer-Coated Surfaces. *Heat Transfer—Asian Research* **1999,** *28*, 551-558.

47. Awaja, F.; Gilbert, M.; Kelly, G.; Fox, B.; Pigram, P. J. Adhesion of Polymers. *Prog. Polym. Sci.* **2009,** *34*, 948-968.

48. Wu, S. Modifications of Polymer Surfaces: Mechanisms of Wettability and Bondability Improvements. *Polymer Interface and Adhesion*, Taylor & Francis Group: New York, 1982; pp 279-336.

49. Comyn, J. Surface Treatment for Adhesion, and for Abhesion. *Adhesion Science*, Royal Society of Chemistry: Cambridge, 1997; pp 18-25.

50. Wen, R.; Xu, S.; Ma, X.; Lee, Y.-C.; Yang, R. Three-Dimensional Superhydrophobic Nanowire Networks for Enhancing Condensation Heat Transfer. *Joule* **2018,** *2*, 269-279.

51. Bustamante, J. G.; Rattner, A. S.; Garimella, S. Achieving Near-Water-Cooled Power Plant Performance with Air-Cooled Condensers. *Appl. Therm. Eng.* **2016,** *105*, 362-371.

52. Rose, J. Some Aspects of Condensation Heat Transfer Theory. *Int. Commun. Heat Mass Transfer* **1988,** *15*, 449-473.

53. Chang, H. C.; Rajagopal, M. C.; Hoque, M. J.; Oh, J.; Li, L.; Li, J.; Zhao, H.; Kuntumalla, G.; Sundar, S.; Meng, Y. Composite Structured Surfaces for Durable Dropwise Condensation. *Int. J. Heat Mass Transfer* **2020**, 119890.

54. Reay, D.; McGlen, R.; Kew, P. Heat Pipe Components and Materials. *Heat Pipes: Theory, Design and Applications*, 6th ed; Butterworth-Heinemann: Oxford, 2014; pp 65-104.

55. Wilke, K. Tailoring Wetting Behavior at Extremes. Doctor of Philosophy, Massachusetts Institute of Technology, Boston, 2019, May 24.

56. Hager, M. D.; Greil, P.; Leyens, C.; van der Zwaag, S.; Schubert, U. S. Self-Healing Materials. *Adv. Mater.* **2010,** *22*, 5424-5430.

57. Blaiszik, B. J.; Kramer, S. L.; Olugebefola, S. C.; Moore, J. S.; Sottos, N. R.; White, S. R. Self-Healing Polymers and Composites. *Annu. Rev. Mater. Res.* **2010,** *40*, 179-211.

58. Morra, M.; Occhiello, E.; Garbassi, F. Wetting Behavior of Oxygen Plasma Treated PTFE. *High Energy Density Technologies in Materials Science*, Kluwer Academic Publishers: Dordrecht, 1990; p 161-168.

59. Yang, M. K.; French, R. H.; Tokarsky, E. W. Optical Properties of Teflon® Af Amorphous Fluoropolymers. *J. Micro/Nanolithogr., MEMS, MOEMS* **2008,** *7*, 033010.

60. McCafferty, E. Validation of Corrosion Rates Measured by the Tafel Extrapolation Method. *Corros. Sci.* **2005,** *47*, 3202-3215.